Femtosecond high-field transport in compound semiconductors

A. Leitenstorfer,* S. Hunsche, J. Shah, M. C. Nuss, and W. H. Knox
Bell Labs, Lucent Technologies, 101 Crawfords Corner Road, Holmdel, New Jersey 07733
(Received 27 August 1999; revised manuscript received 4 February 2000)

A study of nonequilibrium transport of carriers in GaAs and InP at electric fields up to 130 kV/cm and with a temporal resolution of 20 fs is presented. All measurements are carried out at room temperature. The THz radiation originating from the ultrafast current change in a photoexcited semiconductor device is measured by ultrabroadband electro-optic detection. We probe the influences of two important lattice scattering processes on electron acceleration. Distinct differences are seen between GaAs and InP and interpreted in terms of the different band structures and coupling strengths of these important materials. The maximum velocities and carrier displacements achieved under nonequilibrium conditions are measured directly. Peak velocities of 6×10^7 and 8×10^7 cm/s are obtained in GaAs and InP, respectively. The distances achieved during the overshoot regime are found to depend strongly on electric field and material. A displacement as large as 120 nm builds up in less than 200 fs at a field of 60 kV/cm in InP. These findings are important for the design of modern high-speed devices. Coherent excitation of the polar crystal lattice is observed and demonstrated to result from the coupling between free carrier displacement and material polarization via the linear dielectric function. Our experiment is sensitive to collective displacements of the lattice ions with an amplitude as small as 10^{-16} m.

I. INTRODUCTION

The high field transport properties of semiconductors represent a central area in both solid state physics and engineering. From a fundamental point of view, the detailed understanding of the femtosecond dynamics of carriers in an electric field is a key issue in many-body physics. As an example, one may ask whether the well-developed semiclassical picture of electronic conduction breaks down on ultrafast time scales and at very high electric fields.[1] Elements of quantum transport beyond the Boltzmann equation might become significant.[2] In addition, exploring transient high-field transport experimentally is also motivated by the need to obtain information relevant for the design of ultrahigh speed electronics. Quantitative information, e.g., on the length scales connected with non-equilibrium effects, is highly desirable for developing and optimizing devices such as heterojunction bipolar transistors (HBTs) and high-electron mobility transistors (HEMTs).

In the past decade, many experimental studies probing the ultrafast dynamics of the *energy distribution* of electronic excitations in semiconductors have been published.[3] Much less measurement has been carried out to investigate femtosecond transport in high electric fields which is linked to the dynamics of the *momentum distribution* of carriers.[4–11]

Since direct experiments probing nonequilibrium transport on the relevant time scales on the order of 10 fs were missing, this subject had to rely widely on theoretical calculations based on the semiclassical Boltzmann equation.[11–16] To date, related models are in application in the engineering of submicron semiconductor electronics.[17,18]

In this paper, direct and quantitative measurements of the high-field acceleration of free carriers in GaAs and InP with a time resolution of 20 fs are presented. The experiments rely on ultrabroadband electro-optic detection of the THz electromagnetic transients emitted after photoexcitation of charge carriers in a semiconductor material under high electric field. The time resolved THz field amplitude serves as a probe for the momentary charge acceleration in the sample.

A short version of this work has been published recently.[19] The present article contains additional data and a more detailed discussion. It is organized as follows. After the Introduction, a description of the experimental technique is given in Sec. II. Crucial issues, mainly connected to the ultrabroadband nature of the measurements, are discussed. Section III introduces the reader to the fundamental physical processes and concepts which are necessary for a qualitative understanding of transient high-field transport. In Sec. IV, the experimental data are presented and the results are analyzed. The measured THz transients and a qualitative interpretation of the features depending upon electric field and material are contained in Sec. IV A. In the next step (Sec. IV B), the data are corrected for the frequency response of the electro-optic detectors and the quantitative time information is compared to theoretical simulations found in the literature. Section IV C explains the separation of free carrier and lattice contributions to the signals. A method to quantitatively calibrate the measured carrier accelerations, velocities and displacements is described in Sec. IV D and a detailed analysis is added. The observed amplitude of the coherent excitations of the polar crystal lattice is discussed in Sec. IV E. Finally, a conclusion is given in Sec. V.

II. EXPERIMENTAL TECHNIQUE

Our experimental method is based on ultrabroadband detection of the electromagnetic field emitted by accelerating charges. The time resolved electric field amplitude is an ideal probe for ultrafast transport processes since it its proportional to the momentary current change in a photoexcited semiconductor structure.

The experimental setup is depicted schematically in Fig.

0163-1829/2000/61(24)/16642(11)/$15.00 PRB 61 16 642 ©2000 The American Physical Society

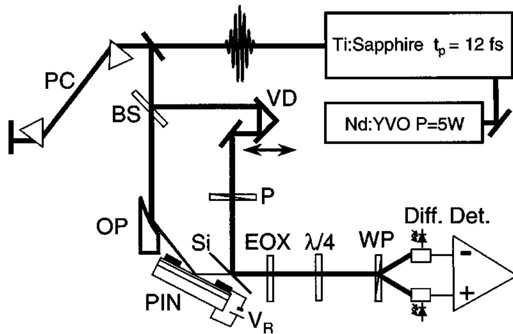

FIG. 1. Experimental setup for the high-field transport measurements. Charge carriers are generated by a 12 fs laser pulse of the Ti:sapphire laser in the reverse biased p-i-n diode (PIN). The emitted THz transient is detected with the help of an electro-optic crystal (EOX). PC: prism compressor for dispersion compensation; BS: beam splitter; VD: variable optical delay; P: polarizer; OP: off-axis paraboloidal mirror; Si: high-resistivity silicon window, Au-coated; λ/4: quarter-wave plate; WP: Wollaston prism; Diff. Det.: differential detector.

1: A frequency doubled cw-Nd:vanadate laser (Nd:YVO) serves as a highly stable and powerful pumping source for a home-built mode-locked Ti:sapphire oscillator.[20] This laser delivers ultrashort light pulses of a duration of 12 fs with a central photon energy of 1.49 eV and a bandwidth of 120 meV at a pulse repetition rate of 82 MHz. Following the resonator, the pulses are sent through a prism compressor (PC) which compensates for the group velocity dispersion of the output coupler and the optical elements in the setup. The laser beam is then divided by a pellicle beam splitter (BS). The transmitted pump pulses are focused with an off-axis paraboloidal (OP) mirror (focal length $f = 50\,\text{mm}$) and directed towards a large-area p-i-n (PIN) diode, the semiconductor THz generator. We have investigated devices based on GaAs ($E_{\text{gap}} = 1.43\,\text{eV}$) and InP ($E_{\text{gap}} = 1.34\,\text{eV}$), two important high-speed materials with the fundamental band gap well matched to the photon spectrum of our excitation pulses. The angle of incidence on the sample is 70° towards the surface normal. The p-i-n device is situated 12 mm before the focus of the convergent pump beam. The diode consists of a 5 nm semitransparent Ti top contact, a 20 nm p^+ region, and a 500 nm high-purity intrinsic zone MBE grown on n^+ substrate. High electric fields can be applied over the intrinsic region by biasing the diode in the reverse direction. All experiments are performed at room temperature ($T = 300\,\text{K}$). The internal field in the diode is determined online via electro-reflectance spectroscopy exploiting the Franz-Keldysh effect[21,22] with the broadband optical pump beam as a sampling source.

A laser power of 15 mW is absorbed over a sample surface of 3 mm times 1 mm. Each pump pulse creates an extremely low density of 5×10^{14} electron-hole pairs per cm^3 in the high-field zone. As a result of the small carrier concentration, screening of the bias field and Coulomb scattering due to the photocarriers are negligible. The low peak intensity of the pump pulses also ensures that THz emission originating from nonresonant optical rectification[23] may be neglected in comparison to the contribution from femtosecond charge transport.

The rapid separation of the photogenerated electrons and holes under the influence of the electric field creates a sheet of Hertzian dipoles. In the far field, the amplitude of the THz radiation emitted by each elementary dipole in the sheet is proportional to the time derivative of the current which is determined by three processes: (i) The femtosecond acceleration of photocarriers in the electric field and their deceleration due to scattering processes, (ii) the dielectric response of the polar crystal lattice reacting on the rapid change of the free carrier displacement, and (iii) a later current drop due to the carriers leaving the intrinsic zone within a few ps. The early parts of the electromagnetic transients are dominated by nonequilibrium transport and contain direct information concerning microscopic phenomena such as electron-phonon scattering mechanisms.

The THz transient is emitted in the direction of the reflected pump light, summing all contributions from the excited elementary dipoles. It passes a high-resistivity Si filter (Si) of a thickness of 500 μm and is detected by an electro-optic crystal (EOX) which is situated at the position of the focus of the reflected excitation beam.

We employ ultrabroadband electro-optic sampling[23,24] to detect the dipole radiation: The electric field of the THz transients induces birefringence in the electro-optic crystal EOX. The difference in refractive index is probed by the portion of the laser pulse reflected at the beam splitter (BS) and coupled collinearly into the THz beam via the Si filter. To enhance the reflectivity of the probe pulse, the Si filter is coated with 4 nm of Au on its rear side.

The data presented in this paper are obtained with two different electro-optic detectors: ⟨110⟩ oriented ZnTe and GaP with a thickness of approximately 8 and 13 μm, respectively. The electro-optic sensors exhibit an individual frequency dependent amplitude and phase response due to the TO lattice resonance (5.3 THz in ZnTe and 11 THz in GaP). The crystals are optically contacted to inactive ⟨100⟩ substrates of a thickness of 200 μm to avoid Fabry-Perot effects.

After the sensor, the probe beam is transmitted through a quarter wave plate (λ/4) and split by a Wollaston prism (WP).[23] The intensity difference $\Delta I/I$ between the polarization components of the probe is proportional to the THz electric field present in the electro-optic crystal. $\Delta I/I$ is analyzed by a shot-noise limited differential detector (Diff. Det.) with a relative sensitivity of $10^{-8}\,\text{Hz}^{-1/2}$. The small signals are monitored with a lock-in amplification scheme based on mechanical chopping of the pump beam at 2 kHz. The temporal information of the THz emission is gained by varying the time difference between excitation of carriers and probing of the field via a variable optical delay stage (VD) with an accuracy of 100 nm, corresponding to a time interval of 0.67 fs. In this way, frequency components of the emitted electromagnetic transients up to 70 THz have been detected.[24]

We have taken great care in designing an experiment that gives direct access to the relative acceleration of photogenerated electrons and holes in a high electric field with a time resolution in the order of 10 fs. This goal is achieved measuring a quantity which is proportional to the momentary electric field amplitude emitted by a single electron-hole pair. In the following, we will discuss the experimental details which are crucial to collect quantitative information on ultrafast carrier transport:

The need for low-density excitation requires large-area

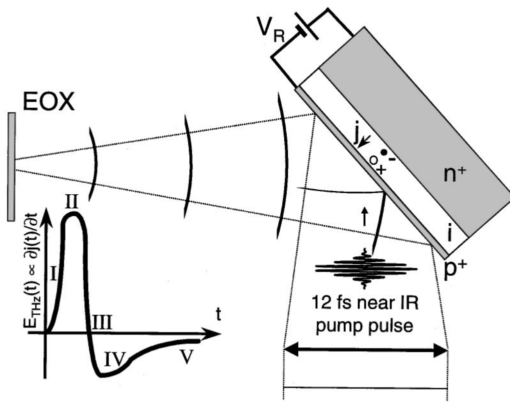

FIG. 2. Schematic geometry to detect the charge acceleration in a large-area p-i-n device. A convergent beam of 12 fs light pulses excites electron-hole pairs in the intrinsic region of a biased diode. The THz electric field amplitude detected in the focal plain of the reflected pump light is proportional to the first time derivative of the diode current j. The different parts (I–V) of the expected THz wave form $E_{\mathrm{THz}}(t)$ are discussed in Sec. III.

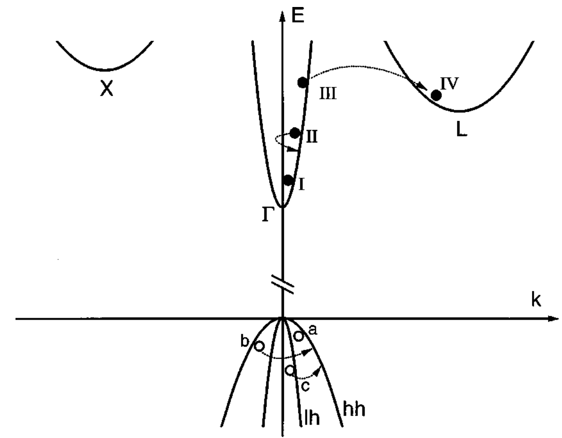

FIG. 3. Scheme of the valence and conduction band structure of GaAs and InP. Electrons are depicted as filled dots, holes as hollow circles. Carrier-phonon scattering processes are indicated with dashed arrows. The denotations are explained in the text.

pumping of a semiconductor sample in order to obtain measurable signals. However, if the electron-hole pairs are generated over an extended region, it has to be ensured that the radiation from each single dipole arrives at the detector EOX with a phase delay smaller than the desired time resolution. The geometrical solution to this problem is sketched in Fig. 2: When the wave front of a collimated laser beam is focused by a parabolic mirror, the path length differences from all points in the original plane wave to the focus are identical. Consequently, when we excite electron-hole pairs in a thin layer before the confocal region, the THz transients emitted by the elementary dipoles in the sheet add up constructively in the focus of the reflected pump light. In addition, the electromagnetic transient has to be detected within an area that is smaller than the diffraction spot of the highest THz frequency relevant for the quantitative analysis of the data. Otherwise, signal components at low frequencies are favored: They allow larger path length differences between generation and detection without destructive interference becoming operative. We work with a diameter of the sampling beam of 100 μm producing negligible errors for frequencies below 50 THz. We want to mention that similar questions have been analyzed in the context of near-field propagation of THz pulses from large-aperture emitter antennas.[25]

Another important issue concerns the sample geometry: It has to be ensured that a double pass of light through the intrinsic region does not disturb the time resolution of the experiment. The optical path through a 500 nm layer with a refractive index of 3.4 is 5 fs. This value is shorter than our time resolution which is limited by the autocorrelation width of the ultrashort laser pulses of approximately 17 fs. The 5 nm Ti cap and the 20 nm p^+ layer do not effect both optical pump beam and infrared emission.

The analysis of the data is straightforward if a situation can be achieved where the dipole radiation pattern is frequency independent and not influenced by the geometry. When free carriers are excited, for example, in the surface field of a dielectric half space[26,27] with a dispersive refractive index, complicated effects arise: The deformation of the dipole lobes[28] strongly reduces THz emission into free space at frequencies where the substrate dielectric function has large values.[27,29] Our sample consists of an extremely thin dielectric layer (the intrinsic zone) on a conducting half space (the n^+ substrate). In this special case, the emission characteristics is identical to a dipole layer situated directly on the surface of a conductor.[30] The radiation lobe coincides with the free space pattern and is independent of frequency.[31] This treatment is valid only in the frequency regime below the plasma resonance of the substrate. The plasma frequency in our samples ($n^+ = 5 \times 10^{18}\,\mathrm{cm}^{-3}$) is approximately 25 THz. In this way, enough bandwidth is provided for a step function response with a rise time of 20 fs.

The THz signal detected in the confocal volume does not correspond to the electron-hole acceleration alone: In any polar material, the ultrafast carrier displacement triggers a coherent response of the crystal lattice[32] which is analyzed and explained in detail in Sec. IV C. As a last point, we recall that the electro-optic signals are to be corrected for the frequency response of the ZnTe and GaP detectors.[24] The amplitude and phase response of the sensors is calculated taking into account reflection and absorption losses, the velocity mismatch between the optical gating pulse and the THz phase and the dispersion of the electro-optic coefficient. A detailed description of the model for the response functions and the correction procedure has been published recently.[24]

III. FUNDAMENTALS OF NONEQUILIBRIUM TRANSPORT

This section introduces the basic physical processes and quantities governing ultrafast transport in direct gap III-V materials and prepares the reader for a qualitative understanding of the experimental data presented in the following.

In Fig. 3, the band structure relevant for the interpretation of our measurements is depicted schematically. The interband transitions induced by the ultrashort excitation pulses create electrons close to the bottom of the Γ valley in the conduction band as well as holes near the top of the valence band. Electrons are depicted as filled dots in Fig. 3 while holes appear as hollow circles. Scattering processes via carrier-phonon interaction are indicated by dashed arrows.

We start with a discussion of the conditions in the conduction band (upper part of Fig. 3): The electrons injected at the Γ point (I) accelerate very efficiently in an applied electric field due to their small effective mass: $m_\Gamma = 0.067 m_0$ and $m_\Gamma = 0.077 m_0$ in GaAs and InP, respectively. In high-purity material and at low excitation densities, the only scattering processes preventing a fully ballistic acceleration are carrier-phonon interactions. Within the Γ valley (II), the dominant coupling mechanism of the electrons to the crystal lattice is polar-optical scattering with longitudinal-optical (LO) phonons. The influence of this Fröhlich-type interaction on high-field transport is quantified by a characteristic electric field E_{Gunn}:[33]

$$E_{\mathrm{Gunn}} = \frac{m_\Gamma e \hbar \omega_{LO}}{4\pi\varepsilon_0 \hbar^2}\left(\frac{1}{\varepsilon_\infty} - \frac{1}{\varepsilon_s}\right) \quad (1)$$

with the LO phonon energy $\hbar\omega_{\mathrm{LO}}$, the high-frequency limit ε_∞, and the static value ε_s of the dielectric constant. This threshold field gives an estimate for the efficiency of momentum relaxation via polar scattering with LO phonons. It coincides approximately with the position of the maximum value of the electron drift velocity in thermal equilibrium since the electrons are still kept within the high-mobility Γ valley. We calculate a value of the Gunn field of 5.3 kV/cm in GaAs and of 15 kV/cm in InP, reflecting the different amount of ionicity in these polar materials.

When an electron in the central valley (III) has gained an energy comparable to the energetic distance between the bottom of the Γ minimum (Γ) and the side valleys in the *L* direction of the Brillouin zone (*L*), very efficient momentum relaxation sets in due to intervalley scattering (IV). These processes occur via deformation potential coupling to various phonon modes at the zone boundary.[34,35] Scattering times are calculated to be less than 20 fs.[16] The energy distance between the Γ and *L* minima is 330 meV in GaAs (Ref. 13) and 860 meV in InP.[36] At very high electric fields, a certain fraction of electrons may reach the *X* valleys of the conduction band (*X*, see Fig. 3) whose energetic separation from the global minimum at the Γ point is even larger [approximately 480 meV in GaAs and 960 meV in InP (Ref. 36)].

The mobility in the satellite valleys is low due to the large effective masses and the strong intervalley scattering. Therefore, in a nonstationary situation (III) where the electrons still accelerate in the Γ minimum, a transient velocity overshoot is expected to occur before a steady-state drift velocity is established in the *L* and *X* minima (IV).

We now turn to the phenomena in the valence bands (lower part of Fig. 3): For our excitation conditions, holes are generated in both the heavy hole (HH) and light hole (LH) bands close to the center of the Brillouin zone. In the central valley of the conduction band, deformation potential scattering with optical phonons is suppressed by the selection rules[37] and acoustic phonon scattering is much less efficient than polar-optical interaction. In contrast, the lower symmetry of the Bloch functions for the valence bands with their *p*-type character allows for deformation potential scattering with phonons of all branches.[37] This fact together with the large density of states in the HH band leads to strong momentum relaxation at the top of the valence band. The total scattering times are calculated to be less than 100 fs at room temperature.[38] When heavy holes are generated in the HH band by the excitation pulse (a), their initial acceleration will be approximately an order of magnitude less than that of the electrons due to the higher effective mass. Heavy holes are likely to scatter within the HH band (b) with an equilibrium drift velocity being established on a time scale of 100 fs. In the case of light holes (c), the initial acceleration should be comparable to the electrons since the effective masses are similar. However, the optical excitation produces by a factor of 3 less holes in the LH band as compared to the HH band. The photogenerated light holes scatter into the HH band with its higher density of states within less than 100 fs, mainly via polar-optical interaction.[38] As a conclusion, the holes are not expected to cause a major contribution to the detected current change in the nonequilibrium regime and the observed signals should be dominated by the electron dynamics in the conduction band.

The qualitative features expected for a THz wave form are sketched in a diagram found in the left part of Fig. 2 where the roman numbers correspond to the electron positions in *k* space (see Fig. 3): When electrons are created close to the Γ point, the emitted field amplitude rises as the time integral of the pump pulse (I). Ballistic acceleration on a time scale short compared to scattering times results in a constant THz amplitude (II). After acceleration, the nonequilibrium peak of the velocity is connected to a zero crossing of the detected transient (III). Next, a strongly negative part of the THz signal is linked to the ultrafast deceleration of the electrons following intervalley transfer (IV). Finally, as the current drops in the diode due to carriers leaving the high-field region, the emitted field remains slightly negative on a time scale of a few ps (V).

IV. EXPERIMENTAL RESULTS AND DISCUSSION

A. Qualitative dependence of the THz transients on electric field and material

The THz signals for GaAs and InP at various electric fields, measured with the 8 μm thick ZnTe detector are depicted in Fig. 1 of Ref. 19. These transients reflect the momentary current change $\partial j/\partial t$ in the p-i-n device after generation of charge carriers with a 12 fs excitation pulse. As pointed out in the qualitative discussion in the previous section, the data are dominated by the electron dynamics: For electric fields E close to the Gunn threshold (5.3 kV/cm in GaAs and 15 kV/cm in InP, see Sec. III), the momentum relaxation due to polar-optical scattering confines most of the electrons into the Γ valley. At low fields of 8 and 12 kV/cm in GaAs and InP, respectively, an acceleration period lasting approximately 350 fs is indicated by the positive THz field [Figs. 1(a) and 1(e) in Ref. 19]. After this time interval, equilibrium drift is established. No indications of a transient velocity overshoot can be resolved. The small negative amplitude at later times is caused by the decrease of current related to carriers leaving the intrinsic region of the p-i-n diodes.

In addition to the time derivative of the free carrier current, the signals reflect the acceleration of the ions in the polar crystal lattice: The rapid displacement of the electron-hole pairs leads to a small but ultrafast change of the internal

electric field. The ion cores start accelerating towards their new equilibrium positions and the polar crystal lattice is excited coherently. As a result, a component oscillating with the LO phonon frequency (8.8 THz in GaAs and 10.3 THz in InP) is superimposed on the signal originating from free carrier transport. The THz emission of these coherent phonons[32] appears very pronounced in the uncorrected data since the amplitude response of the ZnTe electro-optic crystal is enhanced in the frequency regime above the lattice resonance of the detector at 5.3 THz.

When the bias field is increased to 24 kV/cm in GaAs [Fig. 1(b) in Ref. 19], the situation changes significantly and a strong negative signal indicating a fast deceleration of charges appears between 250 and 700 fs: The momentum gain of the electrons from the field is now much stronger than the polar-optical momentum loss and the carriers in the Γ valley reach average velocities substantially above the equilibrium drift (velocity overshoot). Subsequently, the electrons get transferred into the low mobility L and X side minima of the conduction band (Γ to L splitting in GaAs: 330 meV). Consistent with the stronger polar-optical scattering and higher intervalley threshold (860 meV) in InP, the overshoot phenomenon is much less developed at a comparable electric field [Fig. 1(f) in Ref. 19].

At a field of 60 kV/cm, a clear signature of a transient velocity maximum at the zero crossing and a subsequent strong deceleration is also visible in InP [Fig. 1(g) in Ref. 19] and the nonequilibrium features in GaAs become faster [Fig. 1(c) in Ref. 19]. If the initial acceleration and deceleration of the electrons occur within a time scale comparable to the oscillation period of the zone center LO phonon (115 fs in GaAs and 98 fs in InP, respectively), the generation of coherent phonons is resonantly enhanced. This effect is especially pronounced in GaAs at fields above 100 kV/cm [Fig. 1(d) in Ref. 19] because the smaller intervalley threshold energy leads to an earlier deceleration of the electrons than in InP at a comparable field. In addition, the LO oscillation period in GaAs (115 fs) is longer than in InP (98 fs). In both materials, the coherent lattice vibrations decay with a time constant of approximately 5 ps, reflecting the LO phonon dephasing time.

It is interesting to note that the maximum electric field amplitudes in the transients emitted by the p-i-n devices are in the order of 100 V/cm despite the weak optical excitation conditions. This value is estimated taking into account the maximum differential signal $\Delta I/I$ obtained in the experimental data [Fig. 1(d) in Ref. 19], the electro-optic coefficient of the detector material and the thickness of the sensor crystal.

B. Correction for the detector response

On the left hand side of Fig. 4, the THz signals of the GaAs sample are presented for the early time regime and for four different bias fields E. These initial transients are very susceptible to frequency-dependent influences and require special attention. Careful corrections have been performed. The most prominent effect results from the frequency response of the 13 μm GaP electro-optic detector employed for the present measurements: We have calculated the sensor characteristics given by both linear optical effects and the dispersion of the electro-optic coefficient.[24] The corrected accelerations are depicted on the right hand side of Fig. 4.

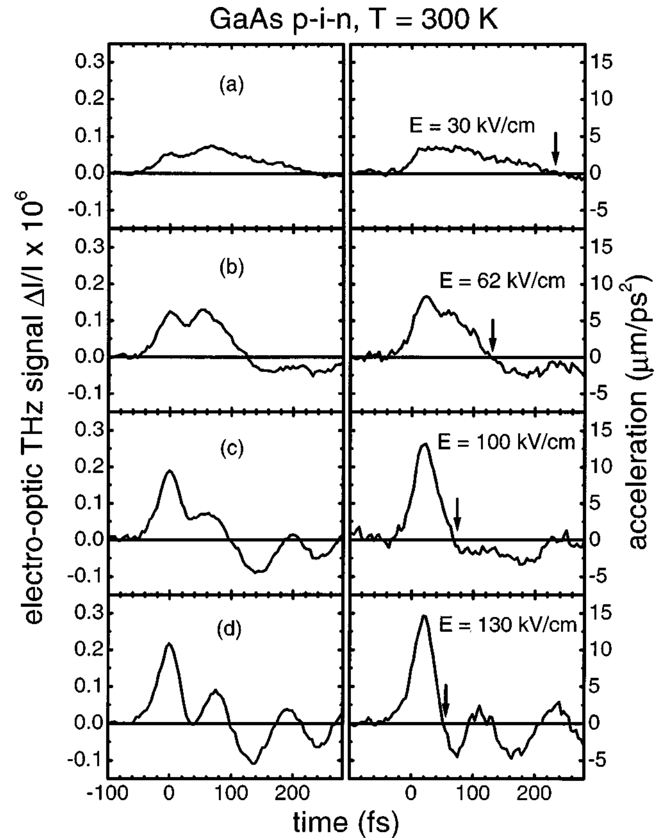

FIG. 4. (a)–(d) Original electro-optic signals (left hand side) and current change corrected for the detector response (right hand side) in a GaAs p-i-n diode for different electric fields E. The measurements are carried out with a GaP electro-optic sensor of a thickness of 13 μm.

The influence of the detector response is seen clearly in Fig. 4(a), comparing the left and right hand sides: The original data (left) exhibit a steplike onset followed by a minimum and an additional maximum with a time delay of roughly 80 fs after the initial rise. This feature turns out to be the result of the dynamic interplay between the electronic and the lattice contributions to the second order nonlinearity of the GaP detector material.[24] The double-peaked structure disappears in the corrected data [right hand side of Fig. 4(a)]: As expected from the instantaneous onset of carrier acceleration, the subtraction of the detector response results in a single step resembling an electromagnetic shock wave. The rise time is given by the time resolution of our experiment of 20 fs. The signal remains constant for approximately 100 fs, indicating a constant acceleration of the carriers over this time interval in GaAs at a bias field of 30 kV/cm.

The corrected data allow an accurate determination of the time it takes to reach the maximum current in the photoexcited p-i-n structure: It is given by the first zero crossing of the THz transients which corresponds to zero average acceleration (marked with arrows in Fig. 4). The maximum velocity is measured to occur after 200 fs at a bias field of 30 kV/cm and after 120 fs at a bias field of 62 kV/cm. These findings are in good agreement with Monte Carlo simulations modeling ultrafast transport of photocarriers within the framework of the semiclassical Boltzmann equation.[15] To our knowledge, the measurements represent the first direct

confirmation for the correctness of a semiclassical description of transport on a time scale of 10 fs.

Theoretical calculations of transient temporal transport at high fields in the order of 100 kV/cm are presently not available in the literature. This regime is especially interesting since the acceleration period in the Γ valley becomes shorter than the oscillation cycle of the zone-boundary optical and acoustic phonons, the scattering partners for intervalley transfer: We find the highest drift velocity to occur after 70 fs at 100 kV/cm and 55 fs at 130 kV/cm. Under these conditions, quantum features such as collisional broadening and intercollisional field effects might significantly influence nonequilibrium transport.[1,2] Nevertheless, an estimate for the time interval to reach the maximum velocity is obtained with the following rate model: If we assume ballistic acceleration of an electron starting at the bottom of the Γ valley, we calculate a lower time limit of 40 fs for the electrons to gain the energy necessary for scattering to the L valley at a field of 130 kV/cm. Since the velocity peaks already 55 fs after excitation, we estimate an extremely short value of 20 fs for the effective transfer time into the side minima. This scattering time compares well with transfer rates calculated via Fermi's golden rule.[16] Our result indicates that a Boltzmann Monte Carlo simulation may be expected to give a reasonable description of transient transport even at electric fields as high as 100 kV/cm. Detailed calculations concerning the intervalley deformation potentials in GaAs and InP may be found in Refs. 34 and 35, respectively. Ultrafast energy relaxation times above the intervalley threshold measured via optical pump-probe spectroscopy[39] also support our findings of extremely efficient momentum redistribution in this regime.

C. Separation of free carrier and lattice contributions

The p-i-n sample may be regarded as a plate capacitor (see Fig. 5) changing its charge on an ultrafast time scale. The region between the conducting plates (the p^+ and n^+ layers) consists of intrinsic GaAs or InP (gray region in Fig. 5). In the state before photoexcitation, the external bias field E_0 gives rise to a sheet density of mesoscopically separated free charges in the doped regions of the sample which is the source for an initial displacement D_0. The intrinsic zone of the diode is an insulating dielectric carrying an induced polarization $P_0 = D_0 - \varepsilon_0 E_0$. The initial polarization P_0 means that the ion cores and the bound electrons of the polar crystal are slightly shifted from their equilibrium positions in a zinc blende lattice without field.

We now proceed to a detailed description of the polarization dynamics after photogeneration of free carriers in the intrinsic semiconductor. At the beginning, we wish to point out three important points the reader should bear in mind throughout this discussion, see Fig. 5: (i) In our system, free charges giving rise to a change in displacement ΔD are generated *inside* the dielectric which is actually a semiconductor. At the same time, the free carrier excitation density N is kept small resulting in a plasma frequency well below the lattice resonance of the system. This limit ensures that the dielectric properties of the intrinsic region remain virtually unchanged with respect to the conditions without excitation. (ii) The free carrier displacement arising inside the intrinsic

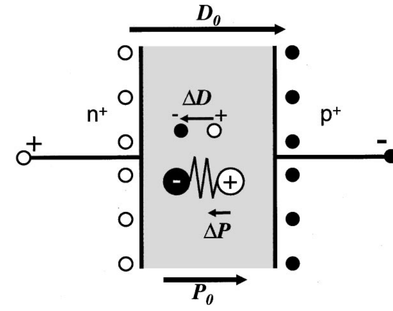

FIG. 5. Schematic sketch of the dynamic interplay between free charge displacement D and material polarization P in the THz emitter. The displacement before photoexcitation and the corresponding induced polarization are denoted by D_0 and P_0, respectively. ΔD is the change in displacement due to the separation of photoexcited carriers and ΔP is the resulting variation of the material polarization. The gray shadowed region corresponds to the high-purity intrinsic zone of the p-i-n diodes. Positive and negative charges are depicted by hollow and filled circles, respectively. The small circles originate from truly separated free charges [(i) situated in the p^+ and n^+ regions due to the external bias field and (ii) photogenerated electron-hole pairs] contributing to the total displacement D. The bound dipole charges of the induced material polarization P are represented by large circles interconnected with a symbolic spring.

zone leads to an ultrafast change of the electric field ΔE, analogous to a partial decharge of the capacitor plates. On the other side, recharging of the system to E_0 by the external bias may be neglected since the RC time constant of the entire circuit is slow (approximately 1 ns). For the fs and ps dynamics discussed in this paper, the capacitor may be regarded as disconnected from the voltage source. The electric field $E(t)$ is determined by the dynamics of the charge distribution inside the p-i-n structure. (iii) The changes in displacement ΔD and thus in bias field occur on such fast time scales that the response of the polarization in the intrinsic region is no longer described by a dielectric constant. Instead, the complex dielectric function $\varepsilon(\omega)$ has to be taken into account over a wide frequency interval in the mid and far infrared spectral regime.

We can now present a quantitative description of the coherent lattice response based on classical electrodynamics of continuous media and in analogy to the capacitor+dielectric problem contained in standard textbooks.[40] After the free carriers have been excited by the ultrashort light pulse, the high electric field E_0 present in the intrinsic zone of the sample leads to a relative acceleration of electrons and holes, as discussed earlier. The rapid carrier separation corresponds to change of the displacement $\Delta D(t)$ (see Fig. 5) which is proportional to the sheet densities of photogenerated charges entering the doped regions

$$\Delta D(t) = Ne\Delta x(t) \tag{2}$$

with the free carrier pair density N and the average distance Δx between electron and hole at a time t after excitation. Since the recharging time by the external bias is slow, $\Delta D(t)$ results in a relatively small but ultrafast screening of the electric field E present in the intrinsic semiconductor region ($\Delta E \leqslant 0.5$ kV/cm within the first 50 fs after excitation, see estimate in Sec. IV E). The ions of the crystal lattice react

accelerating towards their new equilibrium positions. This phenomenon is equivalent to a variation of the dielectric polarization $\Delta P(t)$ (see Fig. 5). Our experimental geometry ensures that the THz electric field $E_{\mathrm{THz}}(t)$ detected at the sampling point reflects the momentary change of the total current density j in the intrinsic region. In turn, $\partial j/\partial t$ is proportional to the second time derivative of the free charge displacement $D(t)=D_0-\Delta D(t)$ minus the dielectric polarization $P(t)=P_0-\Delta P(t)$:

$$E_{\mathrm{THz}}(t)\propto\frac{\partial j}{\partial t}\propto\frac{\partial^2}{\partial t^2}[D(t)-P(t)]. \quad (3)$$

Strictly speaking, P consists of two contributions, from the bound electrons and from the lattice ions: (i) The response of the bound electrons in the dielectric medium may be regarded as instantaneous even on the 10 fs time scale of our experiment. It is represented by a background dielectric constant ε_∞ independent of frequency in the mid and far infrared. (ii) The major contribution to the observed dynamics originates from the ion lattice of the polar semiconductor which has a strong resonance in the frequency regime of interest for ultrafast transport. For this reason, we will talk about the lattice contribution in the following when referring to the dielectric polarization P, keeping in mind that in principle an instantaneous electronic response is present as well. We want to emphasize that Ohm's law, where the current is strictly proportional to the applied electric field, does not hold for the transport phenomena we are studying: First, this relationship is valid only in the steady state whereas we are investigating the extremely transient regime. Second, Ohm's law describes equilibrium transport only in situations with linear response where the momentum relaxation time is independent of electric field. The complicated structure of the conduction band in direct-gap materials leads to highly nonlinear phenomena, e.g., the negative differential resistance above the Gunn field, even under stationary conditions (see Ref. 12).

Figure 6 demonstrates the interplay between free carrier and ionic contributions to the femtosecond charge acceleration. In Fig. 6(a), the original THz signal from the InP emitter at a bias field of 90 kV/cm is shown. This transient has been corrected for the response of the ZnTe electro-optic sensor.[24]

In the frequency domain, $D(\omega)$ and $P(\omega)$ are connected via the frequency-dependent linear dielectric function $\varepsilon(\omega)$:

$$\Delta P(\omega)=(1-\varepsilon(\omega)^{-1})\times\Delta D(\omega). \quad (4)$$

Equation (4) is derived from the definitions for the dielectric polarization $P=\varepsilon_0 E-D$ and for the dielectric function $D=\varepsilon\varepsilon_0 E$ via elimination of the electric field E.[40] Combining Eq. (4) with Eq. (3) transformed into the frequency domain, we see that the spectrum of the electromagnetic transients results from the free carrier displacement renormalized by $\varepsilon(\omega)^{-1}$:

$$E_{\mathrm{THz}}(\omega)\propto\omega^2\times\frac{\Delta D(\omega)}{\varepsilon(\omega)}. \quad (5)$$

The influence of the polar lattice is clearly visible in the Fourier transform of the THz transient: The amplitude spectrum [Fig. 6(b)] is sharply peaked at the LO phonon resonance of InP because the absolute value of the dielectric function has a minimum at this frequency position [Fig. 7(a)]. Consequently, the spectral component of the free carrier acceleration at ν_{LO} is strongly enhanced in the THz emission [Eq. (5)]. In contrast, a minimum amplitude is found at the TO phonon resonance since $|\varepsilon(\omega)|$ exhibits a maximum at ν_{TO} [Fig. 7(a)]. A phase shift of $\Delta\Phi=\pi$ occurs between ν_{TO} and ν_{LO} [Fig. 6(c)]. It is connected to the retarded response of the ion lattice [Fig. 7(b)]. High frequency components of the free carrier motion above ν_{LO} cannot be screened by the polar crystal lattice and do therefore appear relatively enhanced in the amplitude spectrum [dashed gray line in Fig. 6(b)]. However, the lattice polarization is able to follow the electron-hole displacement at frequencies below

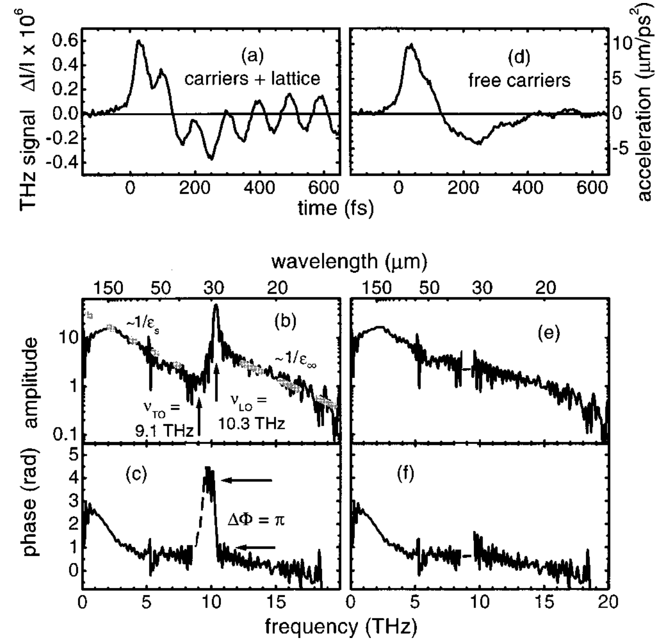

FIG. 6. (a)–(c) Time trace, amplitude, and phase spectrum of the total current change (including the polar lattice, bound electrons, and free carriers) in InP at a bias field of 90 kV/cm. (d)–(f) Free carrier contribution to the signals after correcting for the linear dielectric function of InP.

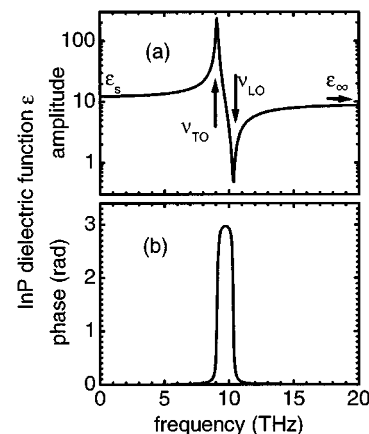

FIG. 7. Absolute value (a) and phase (b) of the dielectric function of InP versus frequency, as calculated with a dielectric oscillator model (Refs. 41 and 42).

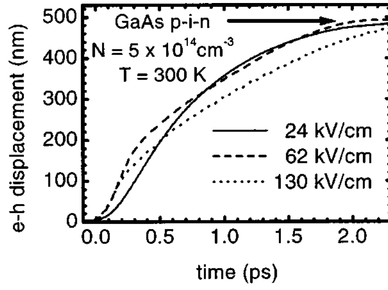

FIG. 8. Total electron-hole displacement versus time in GaAs at different bias electric fields. The horizontal arrow indicates the saturation region related to the maximum electron-hole displacement that can be achieved via carrier drift. To calibrate the data, this plateau value is equated with the width of the high-field region in the *p-i-n* sample of 500 nm.

ν_{TO} [dotted gray line in Fig. 6(b)]. The extrapolated amplitude offset between these two regimes reflects the difference between the high and low frequency limits ε_∞ and ε_s of the dielectric function [see Fig. 7(a)]. In a narrow band around ν_{TO}, our data contain no physical information since the values fall below the noise level [dashed lines in Figs. 6(c), 6(e), 6(f)].

The free carrier contribution to the THz emission is obtained by correcting the amplitude and phase spectra of the original signal with the dielectric function of InP,[41,42] according to Eq. (5). After multiplying the amplitude of $E_{THz}(\omega)$ with the absolute value of $\varepsilon(\omega)$ [Fig. 7(a)] we get a continuous roll-off of the amplitude between 2 and 20 THz [Fig. 6(e)]. The phase shift between the TO and LO frequency is removed by subtracting the argument of the dielectric function [Fig. 7(b)] from the phase spectrum of the THz transient [Fig. 6(f)]. The inverse Fourier transform F^{-1} of the corrected spectra represents the relative acceleration of electrons and holes:

$$\Delta\ddot{D}(t)=Ne\Delta\ddot{x}(t)\propto F^{-1}\{\varepsilon(\omega)\times E_{THz}(\omega)\}. \qquad (6)$$

The result of the transformation back to the time domain may be seen in Fig. 6(d): The oscillatory component of the coherent phonons is almost perfectly removed from the data. Carrier acceleration shows a sharp onset at $t=0$ fs, limited only by the time resolution of the setup. Ballistic transport indicated by constant acceleration takes place for less than 50 fs in InP at 90 kV/cm. As the first carriers start scattering with the crystal lattice, the acceleration decreases towards a zero at 130 fs. At this point, the maximum electron velocity is reached. The electrons then decelerate due to intervalley transfer, as indicated by the negative signal extending to a time delay of 400 fs after excitation.

D. Quantitative data of carrier acceleration, velocity, and displacement

We calibrate our data quantitatively via the following procedure: Integrating the corrected acceleration transients twice in time yields a quantity that is proportional to the average carrier displacement. In Fig. 8, typical integrals are displayed for GaAs at three different bias fields. After a few ps, all carriers have left the intrinsic zone and are stopped very rapidly in the doped regions of the sample. The diffusive transport taking place after the drift period is very slow and does not contribute significantly to the ultrafast THz signals we measure. As a result, all the double integrals saturate at a constant level which turns out to be identical for all electric fields in a given sample (horizontal arrow in Fig. 8). This plateau value is equated with the maximum electron-hole displacement given by the effective width of the high field region of 500 nm (see Fig. 8). In this way, a direct calibration is obtained for the time-dependent carrier displacement and its derivatives, the average velocity and acceleration. The experimental error of the absolute values of acceleration, velocity and displacement is estimated to be less than 25%, largely determined by the noise of the original data entering the double integrals. The accelerations depicted in the right hand side of Fig. 4 are calibrated quantitatively in this way. To our knowledge, the peak value of 16×10^{18} m/s^2 at a field of 130 kV/cm in GaAs ranges among the highest linear accelerations determined so far. The maximum signals below 100 kV/cm are proportional to the electric bias field and equivalent to a ballistic acceleration of a mass of $0.12m_0$. This value is somewhat larger than the reduced mass of an electron-hole pair injected at the band edge which would be $0.06m_0$ assuming an effective electron mass of $m_e=0.067m_0$ and a heavy hole mass of $m_{HH}=0.5m_0$. However, we have to take into account that the central valley of the conduction band may be regarded as parabolic only for relatively small excess energies of the electrons. Assuming a nonparabolicity parameter in the Γ valley of GaAs of $\alpha=0.69$ eV^{-1},[13] an effective mass of approximately $0.1m_0$ is obtained for an energy of 100 meV above the band minimum. We want to mention that somewhat smaller deviations from a parabolic behavior have been obtained in other publications.[43,44] Due to broadband excitation with our ultrashort laser pulses and rapid energy gain of the carriers in the high electric field, a substantial part of the electrons occupies higher states within a time scale shorter than the resolution of our experiment. As a result, the mass values we measure differ from the conditions expected exactly at the band edge. The nonparabolicity of the conduction band also results in a decreasing electron acceleration already during the ballistic regime: The effective mass in the Γ valley close to the intervalley threshold is approximately $0.2m_0$ in GaAs, i.e., three times larger than at the band edge. For this reason, the acceleration at high fields is found to decrease immediately after excitation [right hand side of Figs. 4(b)–4(d)], whereas an approximately constant regime is resolved only at a field of 30 kV/cm [right-hand side of Fig. 4(a)].

In Fig. 9, the acceleration, velocity and displacement of free carriers in InP can be seen as a function of time at 90 kV/cm. Temporal integration of the acceleration data [Fig. 9(a)] results in the relative drift velocity between electron and hole [Fig. 9(b)]. The transient velocity exhibits a distinct maximum originating from the velocity overshoot of the electrons in the Γ valley before they get scattered to the low-mobility side valleys. We note that the observed peak velocity of 8×10^7 cm/s is an order of magnitude higher than the steady-state drift velocity of electrons of 0.8×10^7 cm/s (Ref. 45) at 90 kV/cm. The equilibrium drift velocity for holes at the same field is approximately 1.1×10^7 cm/s.[14,46] As a good check for our calibration procedure, the results for the drift velocity after the initial nonthermal regime [e.g., 2

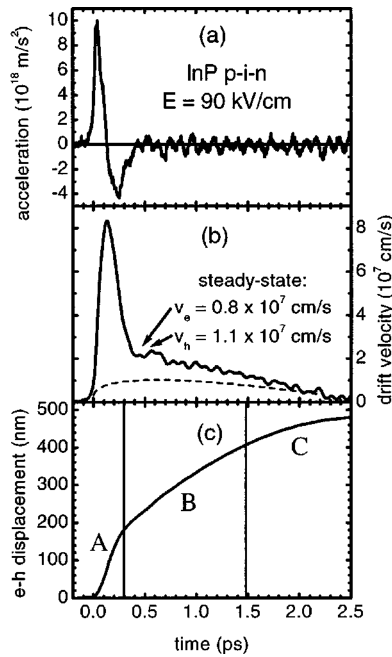

FIG. 9. Carrier acceleration (a), relative drift velocity (b), and electron-hole displacement (c) in InP at a bias field of 90 kV/cm. In Fig. 9(b), the transition to steady-state transport is marked with arrows and the equilibrium drift velocities for electrons and holes found in the literature are given explicitly. The approximate contribution of the hole velocity is indicated qualitatively by the dashed curve.

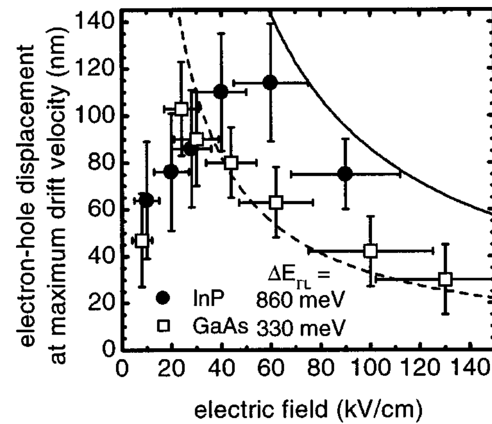

FIG. 10. Carrier displacement reached at the point of maximum drift velocity versus electric field. The drift distances necessary to gain a field energy corresponding to the intervalley threshold $\Delta E_{\Gamma R}$ are depicted for GaAs (dashed line) and InP (solid line), respectively.

$\times 10^7$ cm/s after approximately 0.4 ps in Fig. 9(b)] are in excellent agreement with the sum of the electron and hole steady-state velocities found in the literature.[12] Thus, while the acceleration data are dominated by the effective acceleration and rapid deceleration of electrons [Fig. 9(a)], the quantitative values for the drift velocities in the equilibrium regime give clear evidence for the contribution by the photogenerated holes [Fig. 9(b)]. A qualitative estimate of the hole contribution to the time-dependent relative velocity is represented by the dashed curve in Fig. 9(b). It has to be stressed that the measurement reflects the intrinsic velocities only in the early time regime (less than approximately 1 ps), i.e., before the current drop due to the carriers entering the doped regions becomes significant.

Figure 9(c) displays the corresponding carrier displacement: A strongly nonlinear initial regime (A) is followed by quasiequilibrium drift (B). After approximately 1.5 ps, the distance starts to level off because the amount of carriers having left the drift region becomes large (C).

The maximum drift velocities during the nonequilibrium acceleration are depicted versus electric field in Fig. 5(a) of Ref. 19 for GaAs and InP: We find that the peak velocities in both materials are comparable below 40 kV/cm. At higher fields, InP allows a larger velocity overshoot due to the larger energy splitting between the central and subsidiary minima in the conduction band. In order to estimate the maximum possible drift velocity for the electrons, one has to take into account two effects: (i) Our data include the hole velocity which increases up to approximately 1×10^7 cm/s (Refs. 14 and 39) at the highest fields and which may be attained in less than 100 fs,[38] as sketched by the dashed curve in Fig. 9(b). (ii) Due to the broadband excitation above the band edge, the electrons are reaching the threshold energy for intervalley transfer at slightly different times. Consequently, the maximum velocity of a single electron may be higher than the experimentally measured value which is an average over the entire electron distribution. The slight decrease of the maximum velocities at very high fields and the sublinear increase of the initial acceleration [Fig. 4(d)] in GaAs above 100 kV/cm may be an indication for the onset of phenomena beyond a semiclassical description of carrier transport. But these deviations are small and require a higher accuracy than the present experiment.

Figure 10 displays the electron-hole displacement reached at the point of maximum drift velocity [i.e., the ordinate values at the maximum slopes of the graphs in Figs. 8 and 9(c)] as a function of electric field. For comparison, the field dependent distance necessary for an electron to experience a potential difference in the field equivalent to the intervalley threshold (330 meV in GaAs,[13] dashed line and 860 meV in InP,[36] full line) is shown. At high fields, the data points fit approximately to the calculated curves: The maximum velocity occurs after a transit length close to the distance it takes for the electrons to gain the energy of the Γ-L splitting in both materials. In this regime, the nonequilibrium transport of electrons is dominated by quasiballistic acceleration within the Γ valley followed by extremely efficient momentum redistribution due to interaction with intervalley phonons via the deformation potential. Since the Fröhlich interaction is inversely proportional to the wave vector of the involved phonon,[37] intraband polar optical scattering favors small momentum transfer to the lattice. The collisions occur mainly in the forward direction leading to a negligible role of polar interactions for momentum relaxation at field values much larger than the Gunn threshold. For lower electric fields, the displacement at the maximum velocity becomes much less than the distance equivalent to a potential difference necessary for intervalley transfer: The electrons do not accelerate efficiently enough to overcome polar-optical momentum loss. Interestingly, the transition to a ballistic motion within the Γ valley occurs at substantially different bias fields for the two materials we have studied: Momentum

relaxation due to the interaction with LO phonons within the central valley is important at fields up to 40 kV/cm in InP with its stronger Fröhlich coupling. In contrast, the ultrafast transport in less polar GaAs is dominated exclusively by intervalley processes already for fields above 25 kV/cm. The displacement values at the maximum velocity overshoot are a measure for the dimensions where device operation becomes completely dominated by nonequilibrium effects depending on electric field and material. To our pleasant surprise, we find that the experimental data are in quantitative agreement with theoretical predictions of nonequilibrium spatial transport in GaAs and InP based on Monte Carlo simulations.[13]

E. Amplitude of coherent phonons

In addition to the absolute calibration of the free carrier transport, we can also estimate the coherent displacement of the ion cores quantitatively. To this end, we have performed the following analysis: The THz wave form emitted by the InP p-i-n at a bias field of 90 kV/cm [Fig. 6(a), free carriers+lattice] is integrated twice in time. The result is very similar to the displacement curve in Fig. 9(c), the only difference being a small modulation at the LO phonon frequency superimposed on the data. Analogous to the procedure performed with the pure free carrier data in Fig. 9, we do now attach a value of 500 nm (the width of the intrinsic zone) to the plateau appearing in the double integral after approximately 2.5 ps. We find that the maximum peak to peak amplitude of the phonon oscillations in this data set is $d^* = 1.5\,\mathrm{nm}$. This distance would correspond to the maximum ion displacement, if the oscillation is caused by a movement of elementary charges e with the same density as the photoexcited electron-hole pairs. In order to adapt d^* to the true conditions of the lattice system, we have to take into account that the density of ion pairs in InP of $N_{\mathrm{ion}} = 2 \times 10^{22}\,\mathrm{cm}^{-3}$ is much higher than the electron-hole excitation density of $N = 5 \times 10^{14}\,\mathrm{cm}^{-3}$. A smaller correction comes from the fact that the chemical bond in InP is not purely ionic, the effective charge of the unit cell being $e^* = 0.28e$. The maximum amplitude d of the relative displacement of the positive and negative ions in the crystal lattice is then given by

$$d = \frac{N}{N_{\mathrm{ion}}} \times \frac{e}{e^*} \times d^*. \tag{7}$$

Using the relationship in Eq. (7), it turns out that the maximum amplitude of the coherent phonons we excite in InP at 90 kV/cm is $1.3 \times 10^{-16}\,\mathrm{m}$. This displacement is almost seven orders of magnitude smaller than the lattice constant of $a = 5.9 \times 10^{-10}\,\mathrm{m}$. In fact, it is only a fraction of the diameter of the P nucleus of $d_{\mathrm{nucleus}} = 4 \times 10^{-15}\,\mathrm{m}$. These findings visualize a unique sensitivity of our measurements for collective vibrational motions.

An independent estimate for the maximum amplitude of the coherent phonons induced in the experiment may be performed as follows: From the LO phonon frequency and the reduced mass of the ion pair in the unit cell of InP, we calculate a force constant for the LO phonon harmonic oscillator of $K = 60\,\mathrm{N/m}$.[47] The change in electric field ΔE due to the free carrier displacement is given by

$$\Delta E = \frac{Ne \times \Delta x}{\varepsilon_\infty \varepsilon_0}. \tag{8}$$

Based on the transport data, we estimate a change in electron-hole displacement of $\Delta x = 50\,\mathrm{nm}$ achieved on a time scale short compared to the LO oscillation period at a field of 90 kV/cm. This value corresponds to a quasi-instantaneous screening of the external bias field of $\Delta E = 0.5\,\mathrm{kV/cm}$. The peak-to-peak amplitude d of the relative oscillation between the ions in the unit cell induced by this field step amounts to

$$d = 4 \times \frac{e^* e \times \Delta E}{K}. \tag{9}$$

For the parameters inferred above, we obtain $d = 1.4 \times 10^{-16}\,\mathrm{m}$, in surprising agreement with the experimental results.

V. SUMMARY

In conclusion, a powerful experimental technique giving direct access to the nonequilibrium transport of carriers in semiconductors has been developed. We want to point out that the method is quite general and applicable to any form of directed charge transfer that can be triggered with ultrashort light pulses. We have studied the high-field dynamics in GaAs and InP with an unprecedented time resolution of 20 fs and in a previously unexplored regime of electric fields up to 130 kV/cm. Intraband polar-optical interaction and intervalley transfer via the deformation potential are identified as the two major lattice scattering processes governing femtosecond transport. At very high electric fields, the scattering of electrons within the Γ valley is negligible and momentum relaxation occurs mainly via intervalley processes. Our data indicate that the time constants for intervalley transfer must be extremely short, less than 20 fs. The transition to a purely ballistic acceleration within the central Γ minimum of the conduction band occurs at lower electric fields in GaAs due to its less polar character and weaker Fröhlich interaction with LO phonons. The measurements also provide direct insight into the influence of band structure effects on ultrafast electronic conduction: The peak velocities of $8 \times 10^7\,\mathrm{cm/s}$ in InP are higher than in GaAs ($6 \times 10^7\,\mathrm{cm/s}$) due to the larger energy separation between the central valley and the side minima in the conduction band. At comparable electric fields, the electrons drift longer distances during the nonequilibrium overshoot regime in InP as compared to GaAs. Coherent excitations of the crystal lattice are observed and shown to emerge from the coupling between free carrier displacement and dielectric polarization via the linear dielectric function of the polar materials. The experimental findings are in good agreement with theoretical simulations found in the literature. These results are of major importance for our general understanding of high-field transport and for the engineering of future semiconductor electronics.

ACKNOWLEDGMENTS

We wish to thank G. C. Cho, J. E. Cunningham, T. C. Damen, K. W. Goossen, E. P. Ippen, W. Y. Jan, W. Kaiser, D. M. Tennant, and G. Zhang for many discussions and other valuable contributions. This work was partially supported by the NEDO Femtosecond Technology Project. S. H. acknowledges funding by the Alexander-von-Humboldt foundation.

*Present address: Physik-Department E11, TU München, D-85748 Garching, Germany. Electronic address: aleitens@ph.tum.de

[1] K. K. Thornber, in *Path Integrals and Their Applications in Quantum, Statistical and Solid-State Physics*, edited by G. J. Papadopoulos and J. T. Devreese (Plenum, New York, 1978), p. 359.

[2] See H. Haug and A.-P. Jauho, *Quantum Kinetics in Transport and Optics of Semiconductors* (Springer, Berlin, 1996).

[3] For an overview, see J. Shah, *Ultrafast Spectroscopy of Semiconductors and Semiconductor Nanostructures*, 2nd ed. (Springer, Berlin, 1999).

[4] W. H. Knox, Appl. Phys. A: Solids Surf. **53**, 503 (1991).

[5] W. Sha, J.-K. Rhee, T. B. Norris, and W. J. Schaff, IEEE J. Quantum Electron. **QE28**, 2445 (1992).

[6] J. E. Pedersen, V. G. Lyssenko, J. M. Hvam, P. Uhd Jepsen, S. R. Keiding, C. B. Sjørensen, and P. E. Lindelof, Appl. Phys. Lett. **62**, 1265 (1993).

[7] T. Dekorsy, T. Pfeifer, W. Kütt, and H. Kurz, Phys. Rev. B **47**, 3842 (1993).

[8] H. Heesel, S. Hunsche, H. Mikkelsen, T. Dekorsy, K. Leo, and H. Kurz, Phys. Rev. B **47**, 16 000 (1993).

[9] B. B. Hu, E. A. De Souza, W. H. Knox, J. E. Cunningham, M. C. Nuss, A. V. Kuznetsov, and S. L. Chuang, Phys. Rev. Lett. **74**, 1689 (1995).

[10] P. Uhd Jepsen, R. H. Jacobsen, and S. R. Keiding, J. Opt. Soc. Am. B **13**, 2424 (1996).

[11] E. D. Grann, K. T. Tsen, D. K. Ferry, A. Salvador, A. Botcharev, and H. Morkoc, Phys. Rev. B **56**, 9539 (1997).

[12] See *Hot-Electron Transport in Semiconductors*, edited by L. Reggiani (Springer, Berlin, 1985), and references therein.

[13] K. Brennan and K. Hess, Solid–State Electron. **27**, 347 (1984).

[14] K. Brennan and K. Hess, Phys. Rev. B **29**, 5581 (1984).

[15] G. M. Wysin, D. L. Smith, and A. Redondo, Phys. Rev. B **38**, 12 514 (1988).

[16] M. V. Fischetti, IEEE Trans. Electron Devices **ED38**, 634 (1991).

[17] M. V. Fischetti and S. E. Laux, IEEE Trans. Electron Devices **ED38**, 650 (1991).

[18] See C. Moglestue, *Monte Carlo Simulation of Semiconductor Devices* (Chapman & Hall, London, 1993).

[19] A. Leitenstorfer, S. Hunsche, J. Shah, M. C. Nuss, and W. H. Knox, Phys. Rev. Lett. **82**, 5140 (1999).

[20] M. T. Asaki, C.-P. Huang, D. Garvey, J. Zhou, H. C. Kapteyn, and M. M. Murnane, Opt. Lett. **18**, 977 (1993).

[21] D. E. Aspnes and A. A. Studna, Phys. Rev. B **7**, 4605 (1973).

[22] D. Birkedal, O. Hansen, C. B. Sørensen, K. Jarasunas, S. D. Brorson, and S. R. Keiding, Appl. Phys. Lett. **65**, 79 (1994).

[23] Q. Wu and X.-C. Zhang, Appl. Phys. Lett. **70**, 1285 (1997); **70**, 1784 (1997).

[24] A. Leitenstorfer, S. Hunsche, J. Shah, M. C. Nuss, and W. H. Knox, Appl. Phys. Lett. **74**, 1516 (1999).

[25] E. Budiarto, N.-W. Pu, S. Jeong, and J. Bokor, Opt. Lett. **23**, 213 (1998).

[26] T. Dekorsy, H. Auer, C. Waschke, H. J. Bakker, H. G. Roskos, H. Kurz, V. Wagner, and P. Grosse, Phys. Rev. Lett. **74**, 738 (1995).

[27] M. Tani, R. Fukasawa, H. Abe, S. Matsuura, K. Sakai, and S. Nakashima, J. Appl. Phys. **83**, 2473 (1998).

[28] C. Fattinger and D. Grischkowsky (unpublished).

[29] W. Lukosz and R. E. Kunz, J. Opt. Soc. Am. **67**, 1607 (1977); **67**, 1615 (1977).

[30] W. Lukosz, J. Opt. Soc. Am. **71**, 744 (1981).

[31] A. Sommerfeld, Ann. Phys. (Leipzig) **28**, 665 (1909); **81**, 1135 (1926).

[32] G. C. Cho, W. Kütt, and H. Kurz, Phys. Rev. Lett. **65**, 764 (1990); T. K. Cheng, S. D. Brorson, A. S. Kazeroonian, J. S. Moodera, G. Dresselhaus, M. S. Dresselhaus, and E. P. Ippen, Appl. Phys. Lett. **57**, 1004 (1990).

[33] See E. M. Conwell, *High Field Transport in Semiconductors* (Academic, New York, 1967), p. 155 ff.

[34] S. Zollner, S. Gopalan, and M. Cardona, J. Appl. Phys. **68**, 1682 (1990).

[35] S. Zollner, S. Gopalan, and M. Cardona, Phys. Rev. B **44**, 13 446 (1991).

[36] S. Zollner, U. Schmid, N. E. Christensen, and M. Cardona, Appl. Phys. Lett. **57**, 2339 (1990).

[37] See B. K. Ridley, *Quantum Processes in Semiconductors* (Clarendon, Oxford, 1993), pp. 107 and 114.

[38] R. Scholz, J. Appl. Phys. **77**, 3219 (1995).

[39] J.-Y. Bigot, M. T. Portella, R. W. Schoenlein, J. E. Cunningham, and C. V. Shank, Phys. Rev. Lett. **65**, 3429 (1990).

[40] See, e.g., J. D. Jackson, *Classical Electrodynamics*, 3rd ed. (Wiley, New York, 1999), pp. 153 ff. and 296. Note that in order to be consistent with our treatment, the ε used in this reference has to be replaced by $\varepsilon\varepsilon_0$.

[41] *Handbook of the Optical Constants of Solids*, edited by E. Palik (Academic, New York, 1985).

[42] J. D. Jackson, *Classical Electrodynamics*, 3rd ed. (Wiley, New York, 1999), p. 309.

[43] U. Rössler, Solid State Commun. **49**, 943 (1984).

[44] T. Ruf and M. Cardona, Phys. Rev. B **41**, 10 747 (1990).

[45] T. H. Windhorn, L. W. Cook, M. A. Haase, and G. E. Stillman, Appl. Phys. Lett. **42**, 725 (1983).

[46] V. L. Dalal, A. B. Dreeben, and A. Triano, J. Appl. Phys. **42**, 2864 (1971).

[47] See, e.g., N. W. Ashcroft and N. D. Mermin, *Solid State Physics* (Saunders College Publishing, Fort Worth, 1976), p. 448.